surfaces

MDPI

Review

Thin Epitaxial Ionic Fluoride Films for Electronics Applications

Giulia Giovanelli [1], Mauro Borghi [2], Alessandro Lodi [1], Tibor Grasser [2] and Luca Pasquali [1,3,4,*]

[1] Department of Engineering "Enzo Ferrari", University of Modena and Reggio Emilia, Via Vivarelli 10, 41125 Modena, Italy; giulia.giovanelli@unimore.it (G.G.); alessandro.lodi@unimore.it (A.L.)
[2] Institute for Microelectronics (TU Wien), Gusshausstrasse 27–29, 1040 Vienna, Austria; borghi@iue.tuwien.ac.at (M.B.); grasser@iue.tuwien.ac.at (T.G.)
[3] Department of Physics, University of Johannesburg, Auckland Park 2006, Johannesburg P.O. Box 524, South Africa
[4] CNR-Istituto Officina dei Materiali (IOM), Strada Statale 14, Km. 163.5 in AREA Science Park, Basovizza, 34149 Trieste, Italy
* Correspondence: luca.pasquali@unimore.it

Abstract: The realization of novel electronic devices based on 2D materials, i.e., field-effect transistors, has recently stimulated a renewed interest regarding ultrathin fluoride epitaxial films. Thanks to their chemical and dielectric properties, ionic fluorides could have the potential to be used as insulators in many applications that require high processing control down to the nanoscale. Here we provide a review of some of the principal results that have been achieved in the past decades regarding the controlled growth of epitaxial fluorides on different types of materials relevant for electronics. The aim is to provide a concise summary of the growth modes, crystallinity, film morphologies, and chemical interactions of different types of fluorides on different type of substrates, highlighting the possibilities of applications and the future perspectives.

Keywords: ionic fluorides; thin films; epitaxy

Academic Editors: Gaetano Granozzi and Aleksey Yerokhin

Received: 12 February 2025
Revised: 11 March 2025
Accepted: 25 March 2025
Published: 27 March 2025

Citation: Giovanelli, G.; Borghi, M.; Lodi, A.; Grasser, T.; Pasquali, L. Thin Epitaxial Ionic Fluoride Films for Electronics Applications. *Surfaces* **2025**, *8*, 22. https://doi.org/10.3390/surfaces8020022

1. Introduction

Recently, ultrathin fluoride films have experienced renewed attention for their potential application in modern electronics [1]. A key factor driving this interest is their use as dielectrics in field-effect transistors (FETs) with ultra-small dimensions, particularly those based on transition metal dichalcogenides (TMDs) [1–5].

The use of crystalline insulators, specifically ionic fluorides, offers a promising approach to improving the interface quality in nanoscale electronic devices. It is indeed possible to synthesize chemically inert, self-passivated surfaces free of dangling bonds by using fluorides [6]. Calcium fluoride (CaF_2), for example, stands out not only for its wide band gap and dielectric constant (Table 1), but also because it can be deposited in ultra-high vacuum (i.e., in ultra-pure conditions) down to monolayers, in a controlled manner, through molecular beam epitaxy (MBE). For example, ultrathin CaF_2 layers grown on weakly doped n-Si(111) substrates have been successfully synthesized with almost defect-free crystalline structures. Furthermore, it has been demonstrated recently that epitaxial CaF_2 can be used as an ultrathin gate insulator for 2D devices which employ MoS_2 as the channel material, where the silicon substrate is used as a back-gate electrode and CaF_2 substitutes SiO_2 as the dielectric material [7].

These promising results can be extended, possibly, to the other alkaline earth fluorides, including MgF_2, BaF_2, and SrF_2, due to their permittivity values and wide band gaps [8]. Additionally, rare-earth metal fluorides such as LaF_3, CeF_3, and NdF_3 are also favorable

candidates, as their wafer-scale growth by thermal evaporation has recently been demonstrated at room temperature. These materials have witnessed intense investigation for the development of MoS_2 and WS_2 transistors [9]. The selected relevant properties of some common fluorides are presented in Table 1.

Table 1. Some relevant fluorides with their crystal structure, lattice constant, energy gap, and permittivity [10–12].

Compound	Energy Gap (eV)	Permittivity	Crystal Structure	Lattice Constant (Å)
BaF_2	11.0	7.33	Cubic (Fluorite)	6.2001
CaF_2	12.1	6.76	Cubic (Fluorite)	5.462
MgF_2	>10	5.42	Tetragonal (Rutile)	a = 4.621, c = 3.055
SrF_2	11.2	6.14	Cubic (Fluorite)	5.800

The potential of fluorides as dielectric materials in electronic devices is well established. Historically, they were proposed as insulators in metal–insulator–semiconductor field-effect transistors (MISFETs). Smith et al. [13] first documented the fabrication of metal–epitaxial insulator–semiconductor field-effect transistors (MEISFETs), using MBE for the growth of CaF_2 on $Si(100)$. These *n*-channel MEISFETs were designed on boron-doped $Si(100)$ substrates. However, the devices employed thick CaF_2 layers (600–800 nm) and presented high variable values of leakage current.

Since then, numerous silicon-based devices incorporating fluoride materials have been developed [14,15]. GaAs MISFETs using a single crystalline calcium fluoride insulator layer have been fabricated using a sequential MBE growth approach of CaF_2 on $GaAs(100)$, demonstrating the promising use of these heterostructures in inversion mode operation [16]. Following these pioneering works, further studies explored MISFETs based on GaAs channel materials and CaF_2 as the dielectric material [17], along with evaluations and comparisons of additional heteroepitaxial systems [18].

This review provides a brief, although non-exhaustive summary of almost fifty years of research on ultrathin epitaxial fluoride films, emphasizing advancements in growth techniques, interface formation, crystallinity, morphology, and recent device innovations.

2. Fluorides on Semiconductors

Cubic alkaline earth fluorides, i.e., CaF_2, SrF_2, and BaF_2, share the same fluorite crystal structure. This makes them suitable for epitaxial growth on semiconductors such as Si and GaAs because of their matched lattice parameters. Since ionic fluorides tend to sublimate in molecular form (XF_2), they can be grown in an ultra-high vacuum while preserving the nominal stoichiometry. The (111) surface represents the natural cleavage plane of the cubic fluoride crystals and presents the lowest surface free energy. It consists of F^-–$X2^+$–F^- triple layers, with no net change in electric potential across each tri-layer stack. Since their surface is terminated by fluorine ions, a self-passivation occurs, making the film naturally inert.

2.1. Alkaline Earth Fluorides on Si

CaF_2 and Si have a lattice mismatch of ≈0.6% at room temperature, which increases up to 2.5% at 700 °C. This structural similarity has been considered ideal for the development of MISFETs and has sparked several works on growth mechanisms of CaF_2 on $Si(111)$ [19–22]. Because of the small lattice mismatch, as well as the low surface free energy of $CaF_2(111)$ compared to $Si(111)$, layer-by-layer growth is expected. Growth conditions, however, play an essential role on the overall heterosystem morphology (Figure 1). At substrate temperatures near 200 °C [23], films with type-A orientation are formed, where the film orientation matches that of the substrate. When the growth temperature exceeds

600–800 °C, the films adopt the type-B orientation [24], which is characterized by a 180° rotation about the surface normal [111] axis of the substrate.

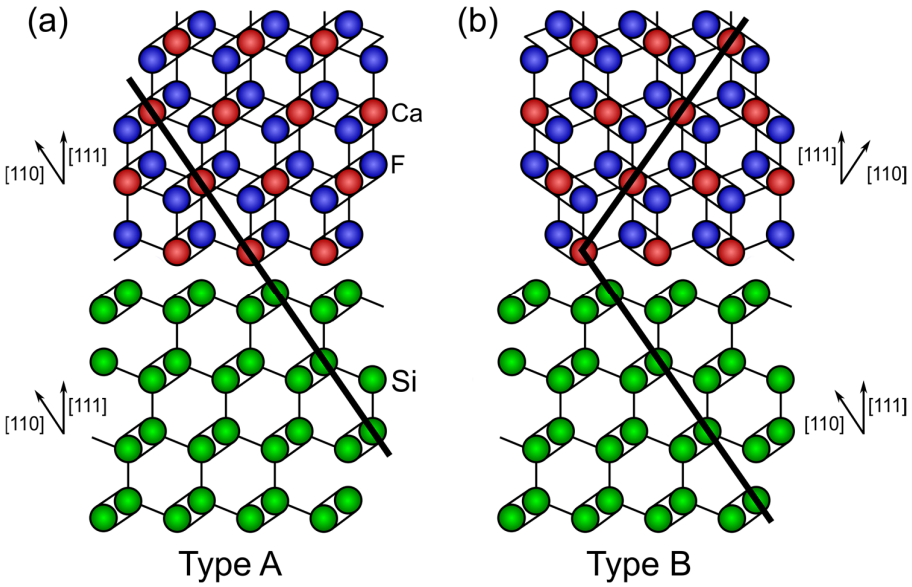

Figure 1. Schemes of the two distinct epitaxial relations at the CaF2/Si(111) interface: (**a**) type-A orientation; (**b**) type-B orientation (adapted from Ref. [25]).

Beyond 600 °C, the thermal energy becomes high enough to drive an interfacial reaction which involves molecular dissociation and the formation of Si–Ca–F bonds. This causes the excess fluorine to be released as volatile SiF_X species that escape from the surface (as shown schematically in Figure 2) [23]. This also favors the formation of a uniform reacted layer that wets the substrate. If the growth temperature is below 600 °C, however, the thermal energy is not sufficient to induce this interface reaction; at around 470 °C, scanning tunnelling microscopy (STM) has demonstrated intact $Si(111) - (7 \times 7)$ regions between 3D CaF_2 islands [26], while at room temperature the formation of single-crystalline layers of CaF_2 is inhibited [23]. These results have also been confirmed by photoemission studies based on surface sensitive core-level spectroscopy [27,28].

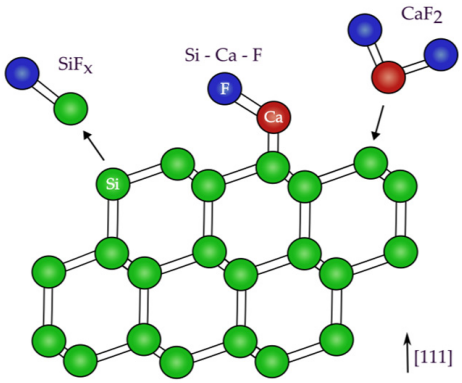

Figure 2. Interface dissociative reaction between CaF_2 and Si occurring at high temperature (adapted from Ref. [23]).

A basic summary of the different growth modes and morphologies that CaF_2 can present on $Si(111)$ is shown in Figure 3, depending on growth parameters such as the substrate temperature and the evaporation rate (flux).

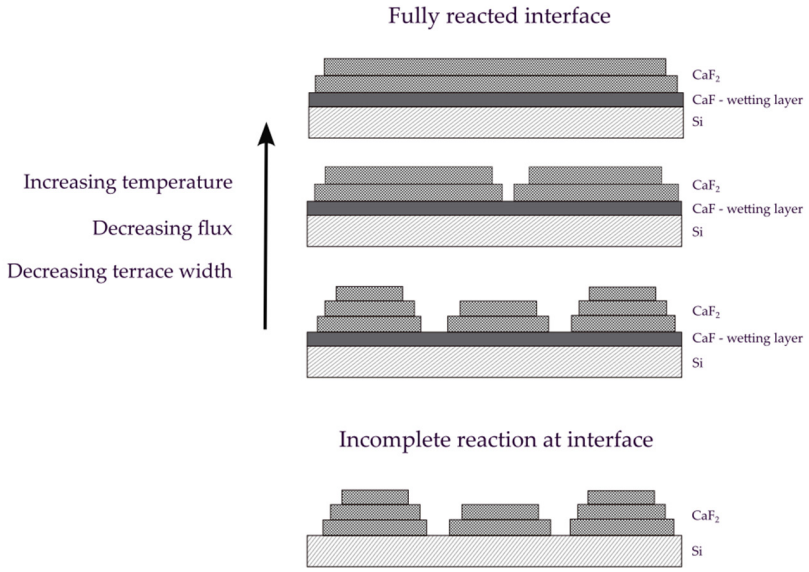

Figure 3. Growth modes and morphologies of the $CaF_2/Si(111)$ system, under different growth conditions. On the top panel, at substrate temperatures above 600 °C during growth, a reacted layer that covers the surface uniformly (i.e., a wetting layer) is formed, on top of which CaF_2 layers and islands develop. On the bottom panel, at low growth temperatures, an incomplete reaction takes place at the interface, with the development of islands that do not uniformly cover (wet) the substrate surface.

Ishiwara et al. [29] studied both the deposition of CaF_2 on Si and the epitaxial growth of interfaces such as Si/insulator/Si by depositing CaF_2 in UHV. They used *p*-type Si wafers with (111) and (001) orientations and examined both the crystallinity and film composition ratios through ion channeling and backscattering. They found that in both cases, the stochiometric ratio of Ca to F was 1:2. Epitaxial growth was observed both on $Si(111)$ and $Si(001)$ at temperatures above 400 °C. The optimal growth temperatures for crystalline structures ranged from 500 °C to 600 °C for $Si(001)$, and from 600 °C to 800 °C for $Si(111)$. The authors also explored the growth of Si onto $CaF_2/Si(111)$, finding that the deposited silicon film also grew epitaxially on the fluoride layer. Moreover, Si growth proved to be less sensitive to O_2 contamination compared to bare Si substrates. Sullivan et al. [30] independently verified these results.

A similar study was carried out on the growth of CaF_2, SrF_2, and BaF_2 on $Si(111)$ and $Si(001)$ [31]. It was found that good-quality SrF_2 and BaF_2 films could be grown at 600 °C on $Si(111)$, and at 400–800 °C on $Si(001)$. Films on $Si(001)$ showed crystallites with (111)-oriented facets. Fathauer et al. [32] further demonstrated that CaF_2 films on $Si(111)$ achieved superior crystalline quality compared to those grown on $Si(001)$. This finding can be attributed to the surface free energy of CaF_2, which is the lowest for (111) surfaces, with respect to (110) and (001) surfaces.

Asano and Ishiwara [33] further concluded that the morphology of the $CaF_2/Si(111)$ system can be controlled by adjusting the growth conditions. X-ray diffraction [24] demonstrated that the type-A orientation is achieved by growing below 400 °C. The role of the deposition rate was also demonstrated to be essential: a slower rate of 0.67 Å s^{-1} led to the formation of epitaxial CaF_2, while working at a much faster rate of 20 Å s^{-1} yielded polycrystalline films. A slower deposition rate allows molecules to remain in contact with the substrate longer, favoring migration to reactive sites and promoting epitaxy.

Strain in MBE-grown CaF_2/Si films, induced by post-deposition cooling due to the large thermal expansion coefficient difference between CaF_2 and Si, is an additional significant aspect to be considered in fluoride growth on silicon [34].

Wong et al. [35] found that the critical thickness for pseudomorphic films grown on Si(111) at a constant temperature of 720 °C is 12 ML, due to the larger lattice mismatch at high temperatures compared to room temperature. It was reported that depositing 6–7 ML of CaF_2 at 720 °C as a template (for subsequent growth at room temperature) can considerably increase the critical thickness. They attributed this layer-by-layer growth at room temperature to the latent heat of condensation of the deposited CaF_2 molecules, which provided the necessary mobility on the $CaF_2(111)$ surface.

In a recent study, Suturin et al. [36] were able to produce uniform and pinhole-free thin layers of CaF_2/Si(111) by keeping the substate temperature at a relatively low value of 250 °C, compared to the other studies reported above, and using a deposition rate of two to three monolayers/s. This allowed them to produce Au/CaF_2/n-Si(111) structures presenting extremely low tunneling currents with a fluoride thickness of 1.5–2 nm.

Compared to Si(111), only a limited number of investigations have focused on CaF_2 growth on Si(001). The clean Si(001) surface is known to reconstruct in a double-domain 2×1 pattern where Si dimers form parallel rows. On adjacent atomic terraces, these rows align along the [110] or $[1\bar{1}0]$ directions, as shown in Figure 4a. Unlike Si(111), which generally supports a layer-by-layer growth mode, Si(001) tends to promote anisotropic nanostructured patterns whose features can be finely tuned through careful control of the growth conditions.

Loretto et al. [37] pioneered efforts to grow elongated CaF_2 islands on Si(001) via MBE. High-resolution TEM revealed two symmetry-equivalent [011] orientations for the CaF_2 islands, each terminated by {111} facets. Sumiya et al. [38] focused on the early stages of CaF_2 growth on Si(100). At room temperature and high coverage, CaF_2 formed small islands that became elongated when annealed at 520 °C, aligning along the silicon [110] and $[1\bar{1}0]$ directions. At 610 °C, these islands evolved into nanostructured layers composed of rows aligned with the substrate, presumably due to a chemical reaction between fluoride and silicon.

Sokolov et al. [39] showed that MBE-grown CaF_2 on Si(001) at 550 °C yielded uniformly spaced, nearly square islands with the same lattice orientation as the substrate. Above 700 °C, however, the fluoride formed nanowires along the [110] and $[1\bar{1}0]$ directions, as indicated by RHEED. These elongated islands formed on top of a one-layer-thick wetting layer. UPS and MDS supported these findings [40]. The interface chemistry was investigated in detail in [41] during CaF_2 deposition on Si(001). An initial ~0.1 monolayer (ML) coverage of CaF_2 at high temperature (770 °C), shown in Figure 4b, produced narrow nanostripes confined to individual terraces and oriented along the [110] and $[1\bar{1}0]$ directions (labeled B and A, respectively). As coverage increased, these nanostripes coalesced into a continuous wetting layer: an example of a terminated wetting layer is shown in Figure 4c (labeled C). Beyond 1 ML, as can be seen in Figure 4d, three-dimensional growth occurred, creating micrometer-length stripes (labeled D) that spanned multiple terraces. The wetting layer is a key factor that governs the orientation of the CaF_2 islands: it is formed by reacted fluoride molecules that undergo dissociation preferentially at the step edges of the Si(001) terraces, leading to volatile SiF_x species that leave the surface and produce a preferential erosion of certain terraces, depending on the orientation of the step edges (see also Figure 2). By selecting appropriate vicinal Si(001) surfaces with a low miscut angle, it is possible to create parallel Si atomic terraces that run closer to either the [110] or $[1\bar{1}0]$ direction, with alternate directions of the dimer rows (Figure 4a) on adjacent terraces. This induces the dissociative erosion reaction to act preferentially on one type of terrace with respect to the other and convert the typical double-domain structure of Si(001) to a single-domain for the dielectric film. Photoemission studies revealed that, under high-temperature and low-coverage conditions, almost complete dissociation of the

fluoride can take place. By contrast, lower-temperature growth (approximately 450 °C) yielded uniformly distributed, rectangular-based CaF_2 islands aligned along the [110] and $[1\bar{1}0]$ directions. Under these conditions, CaF_2 does not wet silicon completely, leaving the substrate uncovered between the islands.

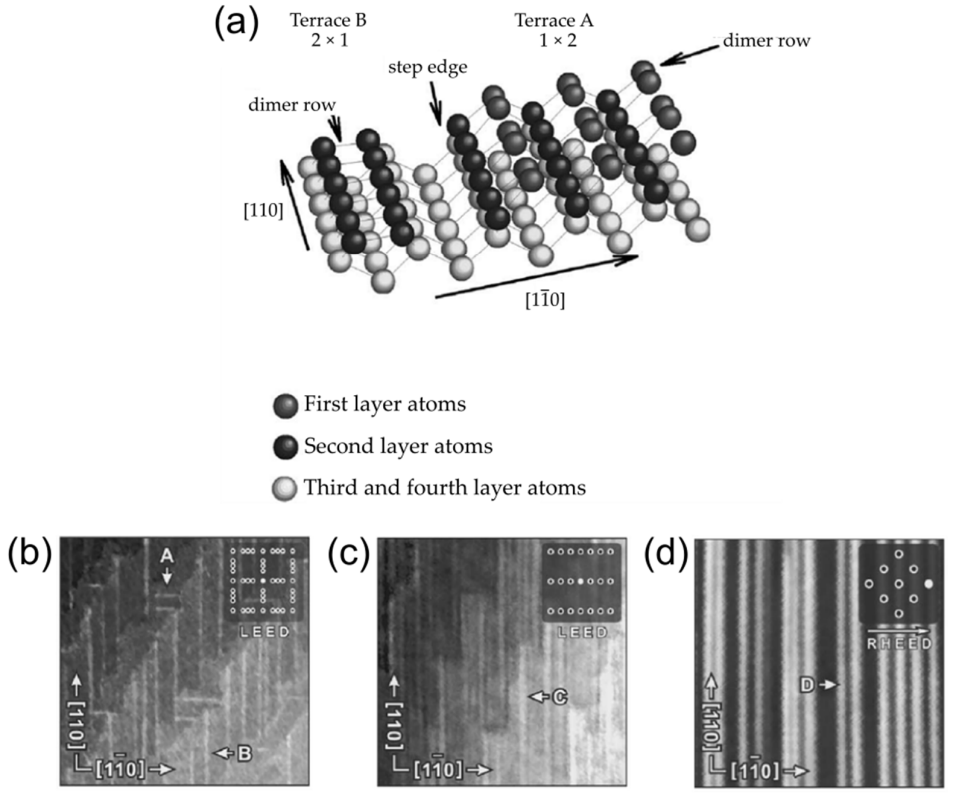

Figure 4. (**a**) Perspective view of the Si(001) double-domain surface. On the bottom, high-temperature (770 °C) deposition of CaF_2 on Si(001): (**b**) 0.1 ML coverage, (**c**) 1 ML coverage, (**d**) 6 ML coverage; the meaning of labels A, B, C and D has been explained in the text (reprinted, with permission, from Ref. [41]. Copyright (2005) by the American Physical Society).

Similarly, MBE-grown SrF_2 on Si(001) was studied in [42], focusing on the interface formation. The results closely resembled the CaF_2 case [41]: at high deposition temperatures (700–750 °C), Figure 5a shows that SrF_2 formed reacted nanostripes running along the [110] or $[1\bar{1}0]$ directions (labeled B and A, respectively). When reaching 1 ML, the nanostripes coalesced into a uniform wetting layer (Figure 5b); for 2–20 ML, 3D islands nucleated on top this interfacial layer (Figure 5c). During the development of the wetting layer, photoemission studies indicated a molecular dissociation and the formation of Sr–Si bonds. At lower deposition temperatures (around 400 °C), flat triangular SrF_2 islands formed without covering the entire surface.

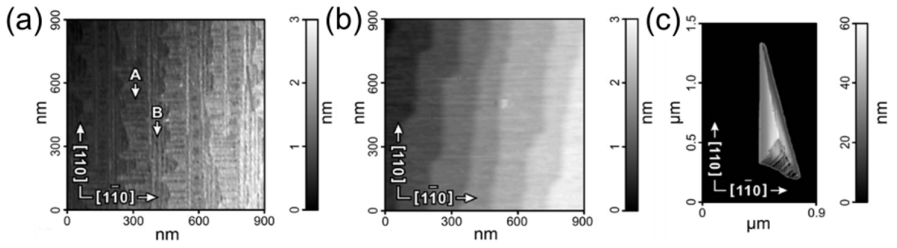

Figure 5. AFM images of SrF_2 grown on Si(001) at 750 °C: (**a**) 0.5 ML coverage, (**b**) 2 ML coverage, and (**c**) 5 ML coverage, with the individual ridge in detail; the meaning of labels A and B has been explained in the text (reprinted, with permission, from Ref. [42]. Copyright (2007) by the American Physical Society).

To provide additional knowledge about growth modes of other fluorides on silicon, beyond the group of alkaline earth metals, Sokolov et al. [39,43] focused on CdF_2 heterostructures. CdF_2 epitaxial layers on Si(111) were fabricated [44], together with CdF_2/CaF_2 superlattices [45]. Calcium fluoride and cadmium fluoride share the same crystal structure, with a low lattice mismatch of 1.4%; CdF_2 shows a band gap value of 8 eV. X-ray diffractometry on CdF_2 directly grown on Si(111) at RT showed poor quality CdF_2 layers; this improved substantially when a buffer layer of CaF_2 was used, and the substrate held at 100 °C. In this case, well-pronounced RHEED specular beam oscillations indicated a 2D growth mode. The growth of CdF_2 on single crystal $CaF_2(111)$ was also tested, which resulted in different morphologies at different deposition temperatures, varying from broad round plateaus separated by CdF_2 single-layer steps (500 °C), well-pronounced faceting resulting in the formation of triangular pyramids (300 °C) and broad triangular plateaus separated by $[1\bar{1}0]$ steps (100 °C).

2.2. Rare-Earth Trifluorides on Si

Rare-earth trifluorides can transform from an orthorhombic to a trigonal structure with increasing temperature. The trigonal phase, having three-fold symmetry, is particularly advantageous for epitaxial growth on (111) surfaces of group IV and III–V semiconductors [46]. Another notable benefit of rare-earth trifluorides is their relatively low thermal expansion coefficients, implying reduced strain during film growth compared to alkaline earth fluorides. Furthermore, unlike group IIA fluorides, rare-earth trifluorides are water-insoluble and feature good mechanical properties.

Sinharoy et al. [47] were the first to report LaF_3 growth on Si(111) in a UHV system at substrate temperatures between 500 and 700 °C. In situ LEED measurements showed a $\sqrt{3} \times \sqrt{3}$ reconstruction for films over 1000 Å thick, confirming that the LaF_3 basal plane was parallel to the Si(111) surface. They also demonstrated that the LaF_3 lattice was rotationally aligned to fit the hexagonal symmetry of the Si(111) cell.

Epitaxial growth of CeF_3 and NdF_3 on Si(111) was reported in [48], maintaining substrate temperatures between 400 and 700 °C. Both CeF_3 and NdF_3 exhibited high-quality epitaxy, though their surface morphologies were highly dependent on temperature. Optimal growth conditions were identified at 600°C for CeF_3 and at 500 °C for NdF_3, producing single-crystalline films. LEED confirmed that the basal planes of the fluorides were parallel to the Si(111) surface, with the film lattice matching the hexagonal structure of silicon.

2.3. Alkaline Earth Fluorides on Ge

Phillips et al. [49] studied the epitaxial growth of BaF_2 on various substrates, including Ge(100) and Ge(111), analyzing the crystalline quality and stoichiometry by Rutherford backscattering and channeling. No epitaxy was observed in the poor lattice-matched BaF_2/Ge(100) system at any temperatures, while the BaF_2/Ge(111) system, despite a very poor lattice matching (9.1%), exhibited good quality, strongly depending on the substrate temperature during the deposition (a better quality was achieved at higher temperatures). This suggests that other factors besides lattice matching contribute to the quality of the epitaxial growth.

The growth of group II fluorides on Ge(111) was reported in [50], focusing on the epitaxial relations between the film and the substrate, investigated through ion channeling and backscattering spectroscopy. The fluorides involved were CaF_2, SrF_2, BaF_2, $Ca_{0.65}Sr_{0.35}F_2$, and $Ca_{0.42}Sr_{0.58}F_2$, evaporated by MBE. The results agreed with the previous research of Phillips et al. [51]: CaF_2, $Ca_{0.65}Sr_{0.35}F_2$, and $Ca_{0.42}Sr_{0.58}F_2$ resulted in a type-B orientation with the substrate, while SrF_2 and BaF_2 resulted in films with both A- and B-type orienta-

tions, with a high lattice strain. It was concluded that these fluorides tend to grow with type-B orientation on non-polar semiconductors.

2.4. Fluorides on III–V Semiconductors

Many efforts have been undertaken regarding the deposition of group II fluorides on III–V semiconductors, such as GaAs, InP, and CdTe. Since these semiconductors crystallize in the zincblende structure, their integration with cubic dielectric materials is particularly interesting due to the low lattice mismatch (lower than 1%), such as, for instance, SrF_2/InP and CaF_2/GaP [52].

Sullivan et al. [53] reported the MBE growth of GaAs/fluoride/GaAs(001) structures using CaF_2 and SrF_2. SrF_2 (~100 Å) was grown at 250–500 °C, and reflection electron diffraction indicated 3D island formation; however, a 1×1 reconstruction was observed after annealing at 400 °C. It was shown that CaF_2 also grew epitaxially on GaAs in the entire range of 250–500 °C. GaAs deposition on both (001) fluorides revealed epitaxial growth in both cases. Nevertheless, strontium fluoride heterostructures showed minimal interlayer diffusion, unlike Ga and As, which diffused into buried CaF_2 layers through cracks caused by the mismatch of both the lattice constant and the thermal expansion coefficient between the GaAs and the fluoride. SrF_2, with a lower elastic constant, better accommodates GaAs, suggesting that mixed fluorides could prevent CaF_2 cracking. Electrical measurements on both films showed good dielectric strength and high resistivity.

The deposition of mixed fluorides has also been reported [50], with lattice-matched $Ca_{0.42}Sr_{0.58}F_2$ films grown on GaAs(111). These films exhibited a type-A orientation, aligning with the substrate's lattice. $Ca_xSr_{1-x}F_2$ was grown on GaAs(001) and GaAs(110) [54]; the composition of the mixed fluoride was chosen to obtain a good lattice matching with GaAs and to take advantage of the similar thermodynamic properties of calcium fluoride and strontium fluoride. Transmission electron diffraction revealed epitaxial growth on (001)- and (110)-oriented GaAs substrates at temperatures above 300 °C; lattice matching was better with the mixed fluoride than with CaF_2.

Mao et al. [55] presented a synchrotron radiation photoemission study of the electronic properties and morphology of the interface between RT-grown CaF_2 and SrF_2 on GaAs(110). Spectra were recorded for the clean substrate and for different nominal coverages, varying from 0.5 to 60 Å; the results suggested the formation of an inert interface between CaF_2 or SrF_2 and GaAs(110) at RT [52].

The growth of BaF_2 and CaF_2 films on InP(001) was studied in [56]. RHEED revealed that BaF_2 growth with the substrate kept at 200 °C resulted in epitaxial layers. BaF_2 was also deposited on CdTe(001) [52], exhibiting again a good epitaxy. At room temperature, electron diffraction demonstrated the presence of polycrystalline BaF_2 films on InP(001) [52], with insufficient surface energy to promote epitaxial growth. Instead, growth at 200 °C resulted in epitaxial films of BaF_2 both on InP(100) and CdTe(100). CaF_2 was deposited on InP(001) at 200 °C and 350 °C: at the lower temperature, the films were polycrystalline, while at the higher temperature, the layers were epitaxial. In this case, RHEED confirmed that the films preserved the same symmetry as the substrate.

Tu et al. [57] realized the first epitaxial III–V semiconductor/dielectric/semiconductor heterostructures, specifically InP/CaF_2/InP(001) and InP/$Ba_xSr_{1-x}F_2$/InP(001). They first grew group II fluorides via MBE on the (001) surface of InP, which presented a 1×2 surface reconstruction. Maintaining the substrate at 500 °C during growth of CaF_2 on a phosphorous-rich surface, RHEED showed a parallel epitaxial relationship between the fluoride and InP(001). Despite the large lattice mismatch between the substrate and the added fluoride (~6.9% at RT), the lattice of InP tended to accommodate the smaller lattice parameter of calcium fluoride, generating a pseudomorphic growth. This behavior is

also attributed to the higher elastic modulus of calcium fluoride with respect to InP. The triple-layer device, with a 100 Å CaF_2 buried film, was then characterized by measuring the current–voltage characteristics at RT; the curves suggested the presence of defects in the film, promoting high leakage currents. The growth of the mixed fluoride [57] reduced the lattice mismatch to ~2%, leading to a better insulator/semiconductor interface and, consequently, substantially reduced charge trapping.

3. Growth of Fluorides on Conductive Substrates

3.1. Fluorides on Metals

Although the growth of fluorides on semiconductors has been widely explored in many past studies, research on metals and conducting materials has been limited. However, this could be of great interest regarding, for instance, the realization of gate contacts.

Farías et al. [58] deposited epitaxial LiF on $Ag(111)$ at low temperature; the first growth stages were investigated through scanning tunnelling microscopy (STM). Performing the deposition at 77 K, it was observed that the fluoride molecules nucleated on both the upper and lower sides of step edges (Figure 6a); this contrasted with metal-on-metal growth, where nucleation typically occurs only on the lower step side. This behavior was attributed to the presence of a strong local electric fields due to charge redistribution at the step sites and parallel to the surface [59,60].

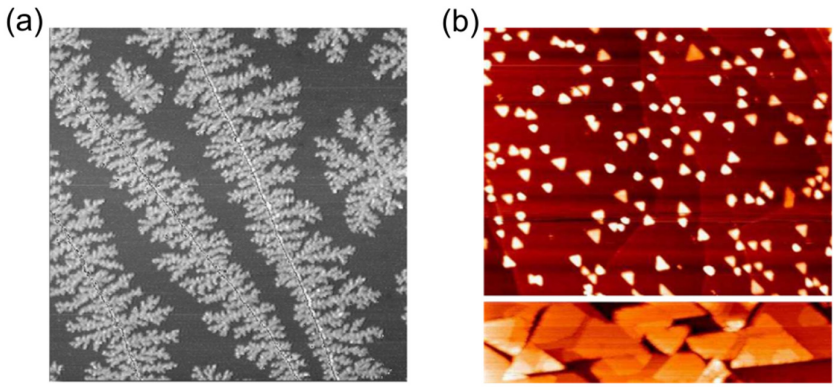

Figure 6. (**a**) STM image taken at 6 K after the deposition of LiF at 77 K, with a deposition rate of 7.3×10^{-4} ML/s (reprinted, with permission, from Ref. [58]. Copyright (2000) by Elsevier). (**b**) On the top, a 500 nm × 500 nm STM image after deposition of 0.4 equivalent TL of CaF_2 on Cu(111) at 900 K. On the bottom, a 500 nm × 140 nm STM image after deposition of 8 TL at 900 K (reprinted, with permission, from Ref. [61]. Copyright (2005) by Elsevier).

The epitaxial growth of $CaF_2(111)$ on $Cu(111)$ at different substrate temperatures was investigated in [61] by STM. The fluoride islands, at temperatures of 400 °C and higher, exhibited triangular shapes in two orientations, rotated 60° relative to each other, with flat top surfaces (Figure 6b). LEED revealed that the films were oriented in the [111] direction and aligned with the substrate. These findings suggested that epitaxial $CaF_2(111)$ twinned crystallites tend to grow on $Cu(111)$.

Borghi et al. [62] studied the deposition of SrF_2 on $Ag(111)$ through MBE in UHV conditions. Specifically, the lattice parameter of SrF_2 is 5.80 Å, while Ag has a lattice parameter of 4.09 Å; however, the mismatch between the metal and SrF_2 is reduced to approximately 0.4% when comparing the spacing between two Ag atoms along the [110] direction with the spacing between two Sr atoms along the [100] direction. Moreover, SrF_2 and Ag share a similar thermal expansion coefficient, around $1.8–1.9 \times 10^{-5}$ K^{-1} at RT. Regarding ultrathin (0.5 nm) layers of SrF_2 deposited at RT, AFM showed a dendritic-like structure (Figure 7a): this morphology was already observed previously [58,61]. RHEED

streak patterns indicated that these SrF_2 islands presented their [111] axis perpendicular to the substrate. At higher coverage, i.e., after a deposition of 1.5 nm, AFM showed that the SrF_2 islands tended to coalesce, leading to a uniform coverage of the substrate at increasing thickness; this was evident at 5 nm at RT, as shown in Figure 7b. A different behavior was obtained at higher temperature deposition: keeping the Ag(111) substrate at 250 °C and depositing 5 nm of fluoride, the surface morphology presented pyramidal shaped islands formed by stacked (111) layers. At 400 °C, similar results were obtained: SrF_2 reorganized on the surface, producing islands with a prismatic shape, which were flat on the top and slightly bigger than those formed at 250 °C (Figure 7c). These islands were made of twinned structures, exhibiting two primary orientations that were rotated 180° relative to each other. XPS indicated that no chemical interface interaction occurred between the Ag and SrF_2, with the preservation of stoichiometry of the bulk fluoride during the deposition, even at the highest substrate temperature.

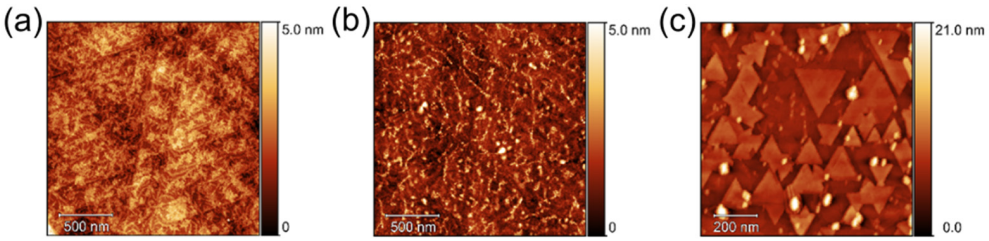

Figure 7. AFM images of SrF_2 grown on Ag(111) at RT: (**a**) 0.5 nm and (**b**) 5 nm of nominal thickness. (**c**) Ex situ AFM image after the deposition of 5 nm of SrF_2 at 400 °C (reprinted from Ref. [62], Creative Commons CC-BY license. Copyright (2024) by Elsevier).

3.2. Fluorides on HOPG

Highly oriented pyrolytic graphite (HOPG) is a non-metallic and conductive material and, when used as a substrate, can be considered somewhat similar to graphene. HOPG has already been the object of many investigations, mainly to grow insulating materials [63–65]. On the other hand, graphene is promising for the development of 2D electronic devices, such as 2D FETs, photodetectors, and even flexible electronic compounds [66,67]. Graphene-based devices require the improvement of stacked heterostructures with 2D oxides or other insulating layers [68,69]. The direct growth of oxides on graphene has proven to be challenging because, due of its low surface energy, it promotes the formation of islands instead of a uniform film. This requires the use of additional treatments, which complicate the deposition process.

Borghi et al. [70] performed the growth of SrF_2 on HOPG through MBE. Growth of SrF_2 on HOPG at RT resulted in the formation of "mosaic islands": small (111)-oriented crystallites were grown slightly rotated around the axis perpendicular to the surface, forming macroscopic dendrites. This was different from the growth mode on Ag [62] or from other metal–fluoride combinations [58,61,71] in which the initial growth phase was characterized by nanometric dendrites (Figure 8a). Even at the nominal thickness of 5 nm, the fluoride did not completely cover the substrate. XPS demonstrated that SrF_2 grew in a bulk-like manner since the very first stages of deposition, with no chemical reaction occurring at the interface. Depositing SrF_2 at higher temperatures changed the surface morphology: at 200 °C, the surface was dominated by star-shaped islands (Figure 8b); at 400 °C, the fluoride tended to accumulate only at the step edges of the substrate terraces, leading to the formation of very long one-dimensional wires (Figure 8c). The self-assembly of very long and almost 1D dielectric wires occurring at 400 °C suggested the intriguing possibility to use MBE for the growth of 1D nanoscale optical guides and dielectric wires.

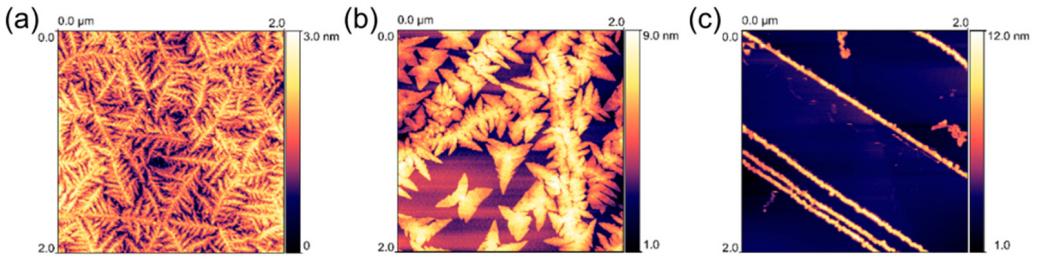

Figure 8. AFM images of SrF_2 growth on HOPG: (**a**) 5 nm of SrF_2 at RT; (**b**) 5 nm of SrF_2 at 200 °C of substrate temperature; (**c**) 5 nm of SrF_2 at 400 °C of substrate temperature (reprinted from Ref. [70], Creative Commons CC-BY license. Copyright (2024) by Elsevier).

4. Perspectives and Future Applications

The intent to use 2D semiconductors in FETs makes it necessary to seek appropriate gate insulator materials.

Miniaturized devices depend on scaled gate insulators with an equivalent oxide thickness (EOT) below 1 nm. Various approaches have been explored, including conventional 3D oxides [72,73] and native oxides of 2D materials [74–76], but both face significant limitations. Amorphous oxides create poorly defined interfaces with multiple dangling bonds [77], resulting in suboptimal subthreshold swings [7,73,78], hysteresis in gate transfer characteristics [79,80] and bias-temperature instabilities [81]. Similarly, the few reported native oxide 2D material stacks exhibit high defect densities, which lead to poor dielectric strengths [82,83]. Intuitively, hexagonal boron nitride (h-BN) could represent a viable option, but studies reported so far have shown that high-quality interfaces must be traded off with unsatisfactory dielectric properties [80,84–87].

Fluorides, particularly calcium fluoride, have been recognized as promising materials. Consequently, CaF_2 has been synthesized using multiple techniques that are scalable for wafer-level fabrication and are applicable to various substrates, with a particular emphasis on Si. In the past, CaF_2 films have already been used as barrier layers in resonant tunneling diodes [88] and superlattices [36].

Several studies have investigated different conductive channels such as graphene [89], silicene [90,91], and black phosphorous [92], while keeping CaF_2 as a dielectric material for digital logic applications. Currently, the focus is on transition metal dichalcogenides (TMDs), i.e., MoS_2, $MoSe_2$, WS_2, etc., two-dimensional materials that exhibit a direct band gap in the monolayer form. TMDs have already been employed for the development of electronic devices, enabling sub-5 nm FET miniaturization [93–95].

Y. Illarionov et al. demonstrated that epitaxial CaF_2 can work in substitution of SiO_2 as an ultrathin gate insulator for 2D devices based on MoS_2 [7]. The fabrication of FETs started with the MBE deposition of a ∼2 nm thick CaF_2 layer onto a clean $Si(111)$ surface at 250 °C. Then, MoS_2 was grown through chemical vapor deposition and transferred onto the CaF_2 substrate. Additional Ti/Au layers were used to contact the channels. Figure 9a shows a schematic sketch of the $CaF_2(111)/MoS_2$ interface formed by F-terminated calcium fluoride and atomically flat MoS_2, while Figure 9b shows the layered structure in the channel area of the device, as obtained with high-resolution TEM. Therefore, heteroepitaxy of 2D materials on a 3D CaF_2 surface was successfully achieved, allowing the interface to be treated as a quasi-van der Waals interface, with minimal defects and dangling bonds. Promising values of on/off current ratios up to 10^7 and subthreshold swing (SS) values below 150 mV/decade were reported in the first prototype devices.

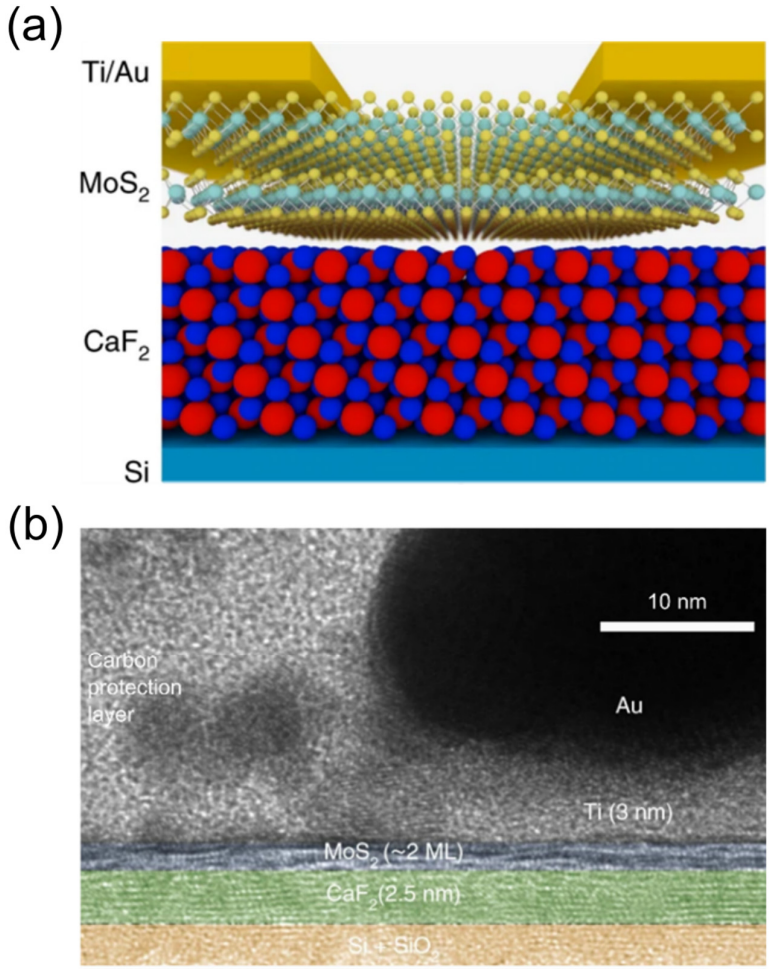

Figure 9. (**a**) Atomistic structure of the quasi-vdW interface between F-terminated $CaF_2(111)$ and MoS_2. (**b**) High-resolution TEM image obtained in the channel area (reprinted from Ref. [7], Creative Commons CC-BY license. Copyright (2020) by Springer Nature).

Das, S. et al. [96] fabricated ~200 n graphene field-effect transistors (GFETs) with a CVD-grown graphene channel and 2 nm of CaF_2 as insulator, examining device variability and hysteresis dynamics. Despite some variability from grain boundaries and CaF_2 imperfections, some nearly identical GFETs were observed. A statistical analysis of hysteresis and bias temperature instability (BTI) up to 175 °C showed that an ambient-sensitive counterclockwise hysteresis was eliminated after annealing. The remaining clockwise hysteresis, linked to CaF_2 border traps, was lower than in GFETs with SiO_2 or Al_2O_3 as gate insulators. Hysteresis was reduced below 0.01 V for an EOT of ~1 nm at high electric fields, meeting commercial standards and confirming CaF_2 as a promising insulator for field-effect devices.

More recently, Meng et al. [9] adopted the thermal evaporation of rare-earth metal fluorides (e.g., LaF_3, CeF_3, NdF_3) to produce *n*- and *p*-type FETs with MoS_2 and WSe_2. Thanks to their strong capacitive coupling at the atomic scale, enhanced by low energy barriers of F^- ion migration in fluorides and a wide bandgap, RE-F_3 films presented a high static dielectric constant (~30 at 10 MHz) and achieved an ultrathin EOT with extremely low leakage currents. Fluoride-gated MoS_2 transistors exhibited nearly ideal subthreshold swing (SS) values, a high on/off current ratio, minimal hysteresis, low gate leakage, low operating voltage, and strong reversibility. The static transfer characteristics of these *n*-type transistors are shown in Figure 10. Meng et al. also integrated *n*-type MoS_2 and *p*-type WSe_2 transistors for the development of CMOS inverter devices, which have been integrated into simple logic circuits.

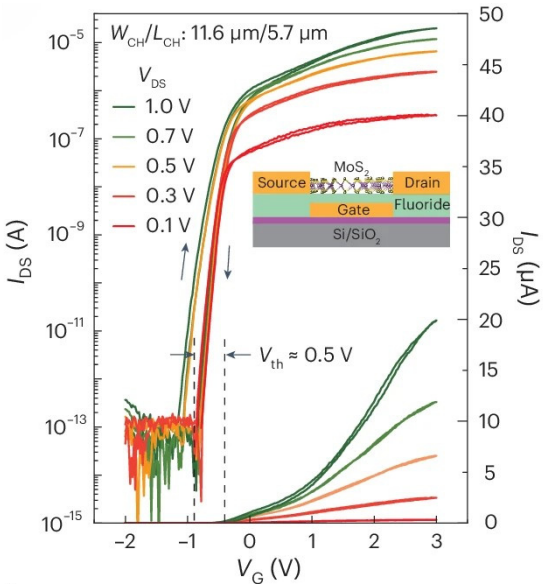

Figure 10. Static transfer characteristics of *n*-type MoS_2 transistors, with a LaF_3 thickness around 100 nm, measured at room temperature with a sweep rate of 100 mV s^{-1}, shown for various VDS values (reprinted, with permission, from Ref. [9]. Copyright (2024) by Springer Nature).

Overall, it may be expected that epitaxial fluorides will be the object of renewed fundamental and technological interest in the next decade, similar to what occurred in the 1980s and 1990s, concerning their growth on "conventional" semiconductors and silicon in particular. To further miniaturize next-generation devices, it is essential to replace silicon oxide and other most common oxides with new insulating materials that are compatible with emerging technologies. Low interaction with 2D semiconductors and conductive contacts, combined with the possible van der Waals nature of the epitaxial layers, makes fluorides dielectrics very promising in nanoelectronics. In addition, the remarkable optical properties, the possibility to introduce controlled luminescence centers by suitable doping [97] in nanoscale-controlled architectures, and the ionic transport capabilities at the nanoscale of different fluorides may open a wide scenario of applications in several fields, including optoelectronics (e.g., nanoscale scintillators [98]), nanoionics and iontronics [99–101] for energy and data storage in miniaturized systems, sensoristics [102,103], and also biofunctionalized materials [104]. On the other hand, much research is still needed to improve the quality and crystallinity of fluoride films on substrates other than conventional semiconductors, and eventually to promote flat-layer growth. Quasi-van der Waals interfaces would be highly desirable for such devices, but a fine control of the chemical composition of the layers and of the defects at the interfaces of the contact and active materials are mandatory steps in order to obtain a reliable and reproducible performance.

Author Contributions: Conceptualization, methodology, resources, data curation, writing—original draft preparation, writing—review and editing, visualization, G.G., M.B., A.L., T.G. and L.P.; supervision, A.L., T.G. and L.P; funding acquisition, A.L., T.G. and L.P. All authors have read and agreed to the published version of the manuscript.

Funding: This research was funded by the European Research Council (ERC) under grant agreement no. 101055379, by the European Commission under the HORIZON-MSCA-2023-PF-01 project CHIMERA, ID 101151367 and the Italian MUR under PRIN 2022 Project 'PETRA', Project n. 2022T7ZSEK, in the frame of Next Generation EU, Mission 4, Component 1, CUP E53D23001860006.

Data Availability Statement: Data sharing is not applicable. No new data were created or analyzed in this study.

Conflicts of Interest: The authors declare no conflicts of interest.

References

1. IRDS. *International Roadmap for Devices and Systems (IRDS)*; IEEE: Piscataway, NJ, USA, 2021; pp. 1–55. Available online: https://irds.ieee.org/editions/2020 (accessed on 1 September 2023).
2. Almutairi, A.A.; Zhao, Y.; Yin, D.; Yoon, Y. Performance Limit Projection of Germanane Field-Effect Transistors. *IEEE Electron. Device Lett.* **2017**, *38*, 673–676. [CrossRef]
3. Akinwande, D.; Huyghebaert, C.; Wang, C.H.; Serna, M.I.; Goossens, S.; Li, L.J.; Wong, H.S.P.; Koppens, F.H.L. Graphene and Two-Dimensional Materials for Silicon Technology. *Nature* **2019**, *573*, 507–518. [CrossRef] [PubMed]
4. Liao, W.; Wei, W.; Tong, Y.; Chim, W.K.; Zhu, C. Electrical Performance and Low Frequency Noise in Hexagonal Boron Nitride Encapsulated $MoSe_2$ Dual-Gated Field Effect Transistors. *Appl. Phys. Lett.* **2017**, *111*, 082105. [CrossRef]
5. Schmidt, M.; Lemme, M.C.; Gottlob, H.D.B.; Driussi, F.; Selmi, L.; Kurz, H. Mobility Extraction in SOI MOSFETs with Sub 1 Nm Body Thickness. *Solid. State Electron.* **2009**, *53*, 1246–1251. [CrossRef]
6. Wen, C.; Lanza, M. Calcium Fluoride as High-k Dielectric for 2D Electronics. *Appl. Phys. Rev.* **2021**, *8*, 021307. [CrossRef]
7. Illarionov, Y.Y.; Banshchikov, A.G.; Polyushkin, D.K.; Wachter, S.; Knobloch, T.; Thesberg, M.; Mennel, L.; Paur, M.; Stöger-Pollach, M.; Steiger-Thirsfeld, A.; et al. Ultrathin Calcium Fluoride Insulators for Two-Dimensional Field-Effect Transistors. *Nat. Electron.* **2019**, *2*, 230–235. [CrossRef]
8. Tomiki, T.; Miyata, T. Optical Studies of Alkali Fluorides and Alkaline Earth Fluorides in VUV Region. *J. Phys. Soc. Jpn.* **1969**, *27*, 658–678. [CrossRef]
9. Meng, K.; Li, Z.; Chen, P.; Ma, X.; Huang, J.; Li, J.; Qin, F.; Qiu, C.; Zhang, Y.; Zhang, D.; et al. Superionic Fluoride Gate Dielectrics with Low Diffusion Barrier for Two-Dimensional Electronics. *Nat. Nanotechnol.* **2024**, *19*, 932–940. [CrossRef]
10. Geyer, R.G.; Baker-Jarvis, J.; Krupka, J. Dielectric characterization of single-crystal LiF, CaF/sub 2/, MgF/sub 2/, BaF/sub 2/, and SrF/sub 2/ at microwave frequencies. In Proceedings of the 17th Annual Meeting of the IEEE Lasers and Electro-Optics Society, 2004, LEOS 2004, Boulder, CO, USA, 20 October 2004; pp. 493–497. [CrossRef]
11. Dorfman, S.M.; Jiang, F.; Mao, Z.; Kubo, A.; Meng, Y.; Prakapenka, V.B.; Duffy, T.S. Phase transitions and equations of state of alkaline earth fluorides CaF_2, SrF_2, and BaF_2 to Mbar pressures. *Phys. Rev. B* **2010**, *81*, 174121. [CrossRef]
12. Rubloff, G.W. Far-Ultraviolet Reflectance Spectra and the Electronic Structure of Ionic Crystals. *Phys. Rev. B* **1972**, *5*, 662–684. [CrossRef]
13. Smith, T.P.; Phillips, J.M.; Augustyniak, W.M.; Stiles, P.J. Fabrication of Metal-Epitaxial Insulator-Semiconductor Field-Effect Transistors Using Molecular Beam Epitaxy of CaF_2 on Si. *Appl. Phys. Lett.* **1984**, *45*, 907–909. [CrossRef]
14. Fathauer, R.W.; Schowalter, L.J. MIS Characterization and Modeling of the Electrical Properties of the Epitaxial CaF_2/Si(111) Interface. *J. Electron. Mater.* **1987**, *16*, 169–175. [CrossRef]
15. Nishioka, Y.; Cho, C.C.; Summerfelt, S.R.; Gnade, B.E.; Brown, G.A. Radiation Characteristics of Epitaxial CaF_2 on Silicon. *IEEE Trans. Nucl. Sci.* **1991**, *38*, 1265–1270. [CrossRef]
16. Waho, T.; Yanagawa, F. A GaAs MISFET Using an MBE Grown CaF_2 Gate Insulator Layer. *IEEE Electron. Device Lett.* **1988**, *9*, 548–549. [CrossRef]
17. Waho, T.; Saeki, H. Electrical Properties of (CaSr)F_2/GaAs(111)B Interfaces Grown by Molecular Beam Epitaxy: Realization of Unpinning. *Jpn. J. Appl. Phys. Takao Waho Saeki* **1991**, *30*, 221–227. [CrossRef]
18. McMullin, P.G.; Sinharoy, S. A Comparative Study of the Electrical Properties of Epitaxial Fluorides. *J. Vac. Sci. Technol. A Vac. Surf. Films* **1988**, *6*, 1367–1370. [CrossRef]
19. Schowalter, L.J.; Fathauer, R.W.; Goehner, R.P.; Turner, L.G.; Deblois, R.W.; Hashimoto, S.; Peng, J.L.; Gibson, W.M.; Krusius, J.P. Epitaxial Growth and Characterization of CaF_2 on Si. *J. Appl. Phys.* **1985**, *58*, 302–308. [CrossRef]
20. Olmstead, M.A.; Uhrberg, R.I.G.; Bringans, R.D.; Bachrach, R.Z. Photoemission Study of Bonding at the CaF_2-on-Si(111) Interface. *Phys. Rev. B* **1987**, *8*, 15. [CrossRef]
21. Lucas, C.A.; Loretto, D.; Wong, G.C.L. Epitaxial Growth Mechanisms and Structure of CaF_2/Si(111). *Phys. Rev. B* **1994**, *50*, 15. [CrossRef]
22. Sokelov, N.S.; Alvarez, J.C.; Yakovlev, N.L. Fluoride Layers and Superlattices Grown by MBE on Si(111): Dynamic RHEED and Sm^{2+} Photoluminescence Studies. *Appl. Surf. Sci.* **1992**, *60*, 421–425. [CrossRef]
23. Olmstead, M.A. *Thin Films: Heteroepitaxial Systems*; Liu, W.K., Santos, M.B., Eds.; World Scientific: Singapore, 1999; pp. 211–266.
24. Cho, C.C.; Liu, H.Y.; Gnade, B.E.; Kim, T.S.; Nishioka, Y. Epitaxial Relations and Electrical Properties of Low-temperature-grown CaF_2 on Si(111). *J. Vac. Sci. Technol. A* **1992**, *10*, 769–774. [CrossRef]
25. Sugiyama, M.; Oshima, M. MBE Growth of Fluorides. *Microelectron. J.* **1996**, *27*, 361–382. [CrossRef]
26. Sumiya, T.; Miura, T.; Tanaka, S. Initial Growth Stage of CaF_2 on Si(111)-7 × 7 Studied by High Temperature UHV-STM. *Surf. Sci.* **1996**, *357–358*, 896–899. [CrossRef]

27. Olmstead, M.A.; Uhrberg, R.I.G.; Bringans, R.D.; Bachrach, R.Z. Initial Formation of the Interface between a Polar Insulator and a Nonpolar Semiconductor: CaF_2 on Si(111). *J. Vac. Sci. Technol. B* **1986**, *4*, 1123–1127. [CrossRef]
28. Himpsel, F.J.; Hillebrecht, F.U.; Hughes, G.; Jordan, J.L.; Karlsson, U.O.; McFeely, F.R.; Morar, J.F.; Rieger, D. Structure and Bonding at the CaF_2/Si (111) Interface. *Appl. Phys. Lett.* **1986**, *48*, 596–598. [CrossRef]
29. Ishiwara, H.; Asano, T. Silicon/Insulator Heteroepitaxial Structures Formed by Vacuum Deposition of CaF_2 and Si. *Appl. Phys. Lett.* **1982**, *40*, 66–68. [CrossRef]
30. Sullivan, P.W.; Cox, T.I.; Farrow, R.F.C.; Jones, G.R.; Gasson, D.B.; Smith, C.S. Growth of Single Crystal and Polycrystalline Insulating Fluoride Films on Semiconductors by Molecular Beam Epitaxy. *J. Vac. Sci. Technol.* **1982**, *20*, 731–732. [CrossRef]
31. Asano, T.; Ishiwara, H.; Kaifu, N. Heteroepitaxial Growth of Group-IIa-Fluoride Films on Si Substrates. *Jpn. J. Appl. Phys.* **1983**, *22*, 1474. [CrossRef]
32. Fathauer, R.W.; Schowalter, L.J. Surface Morphology of Epitaxial CaF_2 Films on Si Substrates. *Appl. Phys. Lett.* **1984**, *45*, 519–521. [CrossRef]
33. Asano, T.; Ishiwara, H. Epitaxial Relations in Group-IIa Fluoride/Si(111) Heterostructures. *Appl. Phys. Lett.* **1983**, *42*, 517–519. [CrossRef]
34. Hashimoto, S.; Peng, J.L.; Gibson, W.M.; Schowalter, L.J.; Fathauer, R.W. Strain Measurement of Epitaxial CaF_2 on Si (111) by MeV Ion Channeling. *Appl. Phys. Lett.* **1985**, *47*, 1071–1073. [CrossRef]
35. Wong, G.C.L.; Loretto, D.; Rotenberg, E.; Olmstead, M.A.; Lucas, C.A. CaF_2-Si(111) as a Model Ionic-Covalent System: Transition from Chemisorption to Epitaxy. *Phys. Rev. B* **1993**, *48*, 5716(R). [CrossRef] [PubMed]
36. Suturin, S.M.; Banshchikov, A.G.; Sokolov, N.S.; Tyaginov, S.E.; Vexler, M.I. Static Current-Voltage Characteristics of Au/CaF_2/*n*-Si(111) MIS Tunneling Structures. *Semiconductors* **2008**, *42*, 1304–1308. [CrossRef]
37. Loretto, D.; Ross, F.M.; Lucas, C.A. Quasi-One-Dimensional CaF_2 Islands Formed on Si(001) by Molecular Beam Epitaxy. *Appl. Phys. Lett.* **1995**, *68*, 2363–2365. [CrossRef]
38. Sumiya, T.; Miura, T.; Fujinuma, H.; Tanaka, S.-I. Surface Reconstruction in CaF_2/Si(001)Investigated by Scanning Tunneling Microscopy. *Surf. Sci.* **1997**, *376*, 192–204. [CrossRef]
39. Sokolov, N.S.; Suturin, S.M. MBE Growth of Calcium and Cadmium Fluoride on Silicon. *Appl. Surf. Sci.* **2001**, *175–176*, 619–628. [CrossRef]
40. Pasquali, L.; D'addato, S.; Selvaggi, G.; Nannarone, S.; Sokolov, N.S.; Suturin, S.M.; Zogg, H. Formation of CaF_2 Nanostructures on Si(001). *Nanotechnology* **2001**, *12*, 403–408. [CrossRef]
41. Pasquali, L.; Suturin, S.M.; Ulin, V.P.; Sokolov, N.S.; Selvaggi, G.; Giglia, A.; Mahne, N.; Pedio, M.; Nannarone, S. Calcium Fluoride on Si(001): Adsorption Mechanisms and Epitaxial Growth Modes. *Phys. Rev. B Condens. Matter.* **2005**, *72*, 045448. [CrossRef]
42. Pasquali, L.; Suturin, S.M.; Kaveev, A.K.; Ulin, V.P.; Sokolov, N.S.; Doyle, B.P.; Nannarone, S. Interface Chemistry and Epitaxial Growth Modes of SrF_2 on Si(001). *Phys. Rev. B* **2007**, *75*, 075403. [CrossRef]
43. Sokolov, N.S.; Suturin, S.M. MBE-Growth Peculiarities of Fluoride (CdF_2-CaF_2) Thin Film Structures. *Thin Solid Films* **2000**, *367*, 112–119. [CrossRef]
44. Kaveev, A.K.; Kyutt, R.N.; Moisseeva, M.M.; Schowalter, L.J.; Shusterman, Y.V.; Sokolov, N.S.; Suturin, S.M.; Yakovlev, N.L. Molecular Beam Epitaxy and Characterization of CdF Layers on CaF (111). *J. Cryst. Growth* **1999**, *201*, 1105–1108. [CrossRef]
45. Sokolov, N.S.; Gastev, S.V.; Khilko, A.Y.; Kyutt, R.N.; Suturin, S.M.; Zamoryanskaya, M.V. CdF_2-CaF_2 Superlattices on Si(111): MBE Growth, Structural and Luminescence Studies. *J. Cryst. Growth* **1999**, *201*, 1053–1056. [CrossRef]
46. Jenkins, L.C.; Griffiths, C.L.; Hughes, A.; Richards, J.; Williams, R.H. Epitaxial Rare Earth Fluoride Insulating Layers on Semiconductors: Structure, Phase Transitions, and Interface Reactions. *J. Vac. Sci. Technol. B* **1993**, *11*, 1541–1545. [CrossRef]
47. Sinharoy, S.; Hoffman, R.A.; Rieger, J.H.; Takei, W.J.; Farrow, R.F.C. Epitaxial Growth of Lanthanide Trifluorides by MBE. *J. Vac. Sci. Technol. B Microelectron. Process. Phenom.* **1985**, *3*, 722–723. [CrossRef]
48. Sinharoy, S.; Hoffman, R.A.; Farrow, R.F.C.; Rieger, J.H. Epitaxial Growth of CeF_3 and NdF_3 on Si(111). *J. Vac. Sci. Technol. A Vac. Surf. Films* **1985**, *3*, 2323–2326. [CrossRef]
49. Phillips, J.M.; Feldman, L.C.; Gibson, J.M.; Mcdonald, M.L. Epitaxial Growth of BaF_2 on Semiconductor Substrates. *Thin Solid Films* **1983**, *18*, 101–107. [CrossRef]
50. Tsutsui, K.; Ishiwara, H.; Asano, T.; Furukawa, S. Epitaxial Relations in Fluoride Films Grown on GaAs(111) and Ge(111) Substrates. *Res. Soc. Symp. Proc.* **1985**, *47*, 93–98. [CrossRef]
51. Phillips, J.M.; Gibson, J.M. The Growth and Characterization of Epitaxial Fluoride Films on Semiconductors. *MRS Online Proc. Libr. (OPL)* **1983**, *25*, 381–391. [CrossRef]
52. Farrow, R.F.C.; Sullivan, P.W.; Williams, G.M.; Jones, G.R.; Cameron, D.C. MBE-Grown Fluoride Films: A New Class of Epitaxial Dielectrics. *J. Vac. Sci. Technol.* **1981**, *19*, 415–420. [CrossRef]
53. Sullivan, P.W.; Bower, J.E.; Metze, G.M. Growth of Semiconductor/Insulator Structures: GaAs/Fluoride/GaAs (001). *J. Vac. Sci. Technol. B Microelectron. Process. Phenom.* **1985**, *3*, 500–507. [CrossRef]

54. Siskos, S.; Fontaine, C.; Munoz-Yague, A. Epitaxial Growth of Lattice-Matched Ca_xSr_1-XF_2 on (100) and (110) GaAs Substrates. *J. Appl. Phys.* **1984**, *56*, 1642–1646. [CrossRef]
55. Mao, D.; Young, K.; Kahn, A.; Zanoni, R.; Mckinley, J.; Margaritondo, G. Photoemission Study of CaF_2-and SrF_2-GaAs(110) Interfaces Formed at Room Temperature. *Phys. Rev. B* **1989**, *39*, 12735. [CrossRef]
56. Sullivan, P.W.; Farrow, R.F.C.; Jones, G.R. Insulating Epitaxial Films of BaF_2, CaF_2 and Ba_xCa_1-XF_2 Grown by MBE on InP Substrates. *J. Cryst. Growth* **1982**, *60*, 403–407. [CrossRef]
57. Tu, C.W.; Forrest, S.R.; Johnston, W.D. Epitaxial InP/Fluoride/InP(001) Double Heterostructures Grown by Molecular Beam Epitaxy. *Appl. Phys. Lett.* **1983**, *43*, 569–571. [CrossRef]
58. Farías, D.; Braun, K.-F.; Fölsch, S.; Meyer, G.; Rieder, K.-H. Observation of a Novel Nucleation Mechanism at Step Edges: LiF Molecules on Ag(111). *Surf. Sci. Lett.* **2000**, *470*, 93–98. [CrossRef]
59. Wandelt, K. The Local Work Function: Concept and Implications. *Appl. Surf. Sci.* **1997**, *111*, 1–10. [CrossRef]
60. Hermann, K.; Gumhalter, B.; Wandelt, K. Perturbation of the Adsorbate Electronic Structure by Local Fields at Surface Defects. *Surf. Sci.* **1991**, *251–252*, 1128–1132. [CrossRef]
61. Calleja, F.; Hinarejos, J.J.; Vázquez De Parga, A.L.; Suturin, S.M.; Sokolov, N.S.; Miranda, R. Epitaxial Growth of CaF_2(111) on Cu(111) Visualized by STM. *Surf. Sci.* **2005**, *582*, 14–20. [CrossRef]
62. Borghi, M.; Mescola, A.; Paolicelli, G.; Montecchi, M.; D'Addato, S.; Vacondio, S.; Bursi, L.; Ruini, A.; Doyle, B.P.; Grasser, T.; et al. Initial Stages of Growth and Electronic Properties of Epitaxial SrF_2 Thin Films on Ag(111). *Appl. Surf. Sci.* **2024**, *656*, 159724. [CrossRef]
63. Sun, Y.; Schouteden, K.; Recaman Payo, M.; Locquet, J.P.; Seo, J.W. Growth and Characterization of Ultrathin Vanadium Oxide Films on HOPG. *Nanomaterials* **2022**, *12*, 3134. [CrossRef]
64. Ahmed, A.S.; Wen, H.; Ohta, T.; Pinchuk, I.V.; Zhu, T.; Beechem, T.; Kawakami, R.K. Molecular Beam Epitaxy Growth of SrO Buffer Layers on Graphite and Graphene for the Integration of Complex Oxides. *J. Cryst. Growth* **2016**, *447*, 5–12. [CrossRef]
65. Cheng, T.S.; Summerfield, A.; Mellor, C.J.; Davies, A.; Khlobystov, A.N.; Eaves, L.; Foxon, C.T.; Beton, P.H.; Novikov, S.V. High-Temperature Molecular Beam Epitaxy of Hexagonal Boron Nitride Layers. *J. Vac. Sci. Technol. B* **2018**, *36*, 02D103. [CrossRef]
66. Lin, Y.-M.; Dimitrakopoulos, C.; Jenkins, K.A.; Farmer, D.B.; Chiu, H.-Y.; Grill, A.; Avouris, P. 100 GHz Transistors from Wafer Scale Epitaxial Graphene. *Science* **2010**, *327*, 662. [CrossRef] [PubMed]
67. Novoselov, K.S.; Geim, A.K.; Morozov, S.V.; Jiang, D.; Zhang, Y.; Dubonos, S.V.; Grigorieva, I.V.; Firsov, A.A. Electric Field Effect in Atomically Thin Carbon Films. *Science* **2004**, *306*, 666–669. [CrossRef]
68. Iannaccone, G.; Bonaccorso, F.; Colombo, L.; Fiori, G. Quantum Engineering of Transistors Based on 2D Materials Heterostructures. *Nat. Nanotechnol.* **2018**, *13*, 183–191. [CrossRef]
69. Geim, A.K.; Grigorieva, I.V. Van Der Waals Heterostructures. *Nature* **2013**, *499*, 419–425. [CrossRef]
70. Borghi, M.; Giovanelli, G.; Montecchi, M.; Capelli, R.; Mescola, A.; Paolicelli, G.; D'Addato, S.; Grasser, T.; Pasquali, L. Comprehensive Study of SrF_2 Growth on Highly Oriented Pyrolytic Graphite (HOPG): Temperature-Dependent van Der Waals Epitaxy. *Appl. Surf. Sci.* **2025**, *680*, 161310. [CrossRef]
71. Candia, A.E.; Gómez, L.; Vidal, R.A.; Ferrón, J.; Passeggi, M.C.G. An STM and Monte Carlo Study of the AlF_3 Thin Film Growth on Cu(111). *J. Phys. D Appl. Phys.* **2015**, *48*, 265305. [CrossRef]
72. Park, J.H.; Fathipour, S.; Kwak, I.; Sardashti, K.; Ahles, C.F.; Wolf, S.F.; Edmonds, M.; Vishwanath, S.; Xing, H.G.; Fullerton-Shirey, S.K.; et al. Atomic Layer Deposition of Al_2O_3 on WSe_2 Functionalized by Titanyl Phthalocyanine. *ACS Nano* **2016**, *10*, 6888–6896. [CrossRef]
73. Li, W.; Zhou, J.; Cai, S.; Yu, Z.; Zhang, J.; Fang, N.; Li, T.; Wu, Y.; Chen, T.; Xie, X.; et al. Uniform and Ultrathin High-κ Gate Dielectrics for Two-Dimensional Electronic Devices. *Nat. Electron.* **2019**, *2*, 563–571. [CrossRef]
74. Chamlagain, B.; Cui, Q.; Paudel, S.; Cheng, M.M.C.; Chen, P.Y.; Zhou, Z. Thermally Oxidized 2D TaS_2 as a High-κ Gate Dielectric for MoS_2 Field-Effect Transistors. *2D Mater.* **2017**, *4*, 031002. [CrossRef]
75. Mleczko, M.J.; Zhang, C.; Lee, H.R.; Kuo, H.-H.; Magyari-Köpe, B.; Moore, R.G.; Shen, Z.-X.; Fisher, I.R.; Nishi, Y.; Pop, E. $HFSe_2$ and $ZrSe_2$: Two-Dimensional Semiconductors with Native High-k Oxides. *Sci. Adv.* **2017**, *3*, e1700481. [CrossRef]
76. Peimyoo, N.; Barnes, M.D.; Mehew, J.D.; De Sanctis, A.; Amit, I.; Escolar, J.; Anastasiou, K.; Rooney, A.P.; Haigh, S.J.; Russo, S.; et al. Laser-Writable High-k Dielectric for van Der Waals Nanoelectronics. *Sci. Adv.* **2019**, *5*, 906–924. [CrossRef] [PubMed]
77. Lemme, M.C.; Echtermeyer, T.J.; Baus, M.; Kurz, H. A Graphene Field-Effect Device. *IEEE Electron. Device Lett.* **2007**, *28*, 282–284. [CrossRef]
78. Illarionov, Y.Y.; Smithe, K.K.H.; Waltl, M.; Knobloch, T.; Pop, E.; Grasser, T. Improved Hysteresis and Reliability of MoS_2 Transistors with High-Quality CVD Growth and Al_2O_3 Encapsulation. *IEEE Electron. Device Lett.* **2017**, *38*, 1763–1766. [CrossRef]
79. Di Bartolomeo, A.; Genovese, L.; Giubileo, F.; Iemmo, L.; Luongo, G.; Foller, T.; Schleberger, M. Hysteresis in the Transfer Characteristics of MoS_2 Transistors. *2D Mater.* **2018**, *5*, 015014. [CrossRef]
80. Vu, Q.A.; Fan, S.; Lee, S.H.; Joo, M.K.; Yu, W.J.; Lee, Y.H. Near-Zero Hysteresis and near-Ideal Subthreshold Swing in h-BN Encapsulated Single-Layer MoS_2 Field-Effect Transistors. *2D Mater.* **2018**, *5*, 031001. [CrossRef]

81. Grasser, T. *Bias Temperature Instability for Devices and Circuits*; Springer Science & Business Media: Cham, Switzerland, 2013.
82. Vexler, M.I.; Tyaginov, S.E.; Illarionov, Y.Y.; Sing, Y.K.; Shenp, A.D.; Fedorov, V.V.; Isakov, D.V. A General Simulation Procedure for the Electrical Characteristics of Metal-Insulator-Semiconductor Tunnel Structures. *Semiconductors* **2013**, *47*, 686–694. [CrossRef]
83. Register, L.F.; Rosenbaum, E.; Yang, K. Analytic Model for Direct Tunneling Current in Polycrystalline Silicon-Gate Metal-Oxide-Semiconductor Devices. *Appl. Phys. Lett.* **1999**, *74*, 457–459. [CrossRef]
84. Lee, G.H.; Yu, Y.J.; Cui, X.; Petrone, N.; Lee, C.H.; Choi, M.S.; Lee, D.Y.; Lee, C.; Yoo, W.J.; Watanabe, K.; et al. Flexible and Transparent MoS_2 Field-Effect Transistors on Hexagonal Boron Nitride-Graphene Heterostructures. *ACS Nano* **2013**, *7*, 7931–7936. [CrossRef]
85. Lee, C.; Rathi, S.; Khan, M.A.; Lim, D.; Kim, Y.; Yun, S.J.; Youn, D.H.; Watanabe, K.; Taniguchi, T.; Kim, G.H. Comparison of Trapped Charges and Hysteresis Behavior in HBN Encapsulated Single MoS_2 Flake Based Field Effect Transistors on SiO_2 and HBN Substrates. *Nanotechnology* **2018**, *29*, 335202. [CrossRef] [PubMed]
86. Illarionov, Y.Y.; Rzepa, G.; Waltl, M.; Knobloch, T.; Grill, A.; Furchi, M.M.; Mueller, T.; Grasser, T. The Role of Charge Trapping in MoS_2/SiO_2 and MoS_2/HBN Field-Effect Transistors. *2D Mater.* **2016**, *3*, 035004. [CrossRef]
87. Knobloch, T.; Illarionov, Y.Y.; Ducry, F.; Schleich, C.; Wachter, S.; Watanabe, K.; Taniguchi, T.; Mueller, T.; Waltl, M.; Lanza, M.; et al. The Performance Limits of Hexagonal Boron Nitride as an Insulator for Scaled CMOS Devices Based on Two-Dimensional Materials. *Nat. Electron.* **2021**, *4*, 98–108. [CrossRef]
88. Watanabe, S.; Maeda, M.; Sugisaki, T.; Tsutsui, K. Fluoride Resonant Tunneling Diodes on Si Substrates Improved by Additional Thermal Oxidation Process. *Jpn. J. Appl. Phys. Part 1 Regul. Pap. Short Notes Rev. Pap.* **2005**, *44*, 2637–2641. [CrossRef]
89. Guerriero, E.; Pedrinazzi, P.; Mansouri, A.; Habibpour, O.; Winters, M.; Rorsman, N.; Behnam, A.; Carrion, E.A.; Pesquera, A.; Centeno, A.; et al. High-Gain Graphene Transistors with a Thin AlO_x Top-Gate Oxide. *Sci. Rep.* **2017**, *7*, 2419. [CrossRef]
90. Tao, L.; Cinquanta, E.; Chiappe, D.; Grazianetti, C.; Fanciulli, M.; Dubey, M.; Molle, A.; Akinwande, D. Silicene Field-Effect Transistors Operating at Room-Temperature. *Nat. Nanotechnol.* **2015**, *10*, 227–231. [CrossRef]
91. Nazzari, D.; Genser, J.; Ritter, V.; Bethge, O.; Bertagnolli, E.; Grasser, T.; Weber, W.M.; Lugstein, A. Epitaxial Growth of Crystalline CaF_2 on Silicene. *ACS Appl. Mater. Interfaces* **2022**, *14*, 32675–32682. [CrossRef]
92. Li, L.; Yu, Y.; Ye, G.J.; Ge, Q.; Ou, X.; Wu, H.; Feng, D.; Chen, X.H.; Zhang, Y. Black Phosphorus Field-Effect Transistors. *Nat. Nanotechnol.* **2014**, *9*, 372–377. [CrossRef]
93. Wu, F.; Tian, H.; Shen, Y.; Hou, Z.; Ren, J.; Gou, G.; Sun, Y.; Yang, Y.; Ren, T.L. Vertical MoS_2 Transistors with Sub-1-Nm Gate Lengths. *Nature* **2022**, *603*, 259–264. [CrossRef]
94. Gong, Y.; Lin, Z.; Ye, G.; Shi, G.; Feng, S.; Lei, Y.; Elías, A.L.; Perea-Lopez, N.; Vajtai, R.; Terrones, H.; et al. Tellurium-Assisted Low-Temperature Synthesis of MoS_2 and WS_2 Monolayers. *ACS Nano* **2015**, *9*, 11658–11666. [CrossRef]
95. Wang, Q.H.; Kalantar-Zadeh, K.; Kis, A.; Coleman, J.N.; Strano, M.S. Electronics and Optoelectronics of Two-Dimensional Transition Metal Dichalcogenides. *Nat. Nanotechnol.* **2012**, *7*, 699–712. [CrossRef] [PubMed]
96. Das, S.; Sebastian, A.; Pop, E.; McClellan, C.J.; Franklin, A.D.; Grasser, T.; Knobloch, T.; Illarionov, Y.; Penumatcha, A.V.; Appenzeller, J.; et al. Transistors Based on Two-Dimensional Materials for Future Integrated Circuits. *Nat. Electron.* **2021**, *4*, 786–799. [CrossRef]
97. Lian, H.; Liu, J.; Ye, Z.; Shi, C. Synthesis and Photoluminescence Properties of Erbium-Doped BaF_2 Nanoparticles. *Chem. Phys. Lett.* **2004**, *386*, 291–294. [CrossRef]
98. Wojtowicz, A.J. Rare-Earth-Activated Wide Bandgap Materials for Scintillators. *Nucl. Instrum. Methods Phys. Res. A* **2002**, *486*, 201–207. [CrossRef]
99. Maier, J. Nanoionics: Ion Transport and Electrochemical Storage in Confined Systems. *Nat. Mater.* **2005**, *4*, 805–815. [CrossRef]
100. Waser, R.; Aono, M. Nanoionics-Based Resistive Switching Memories. *Nat. Mater.* **2007**, *6*, 833–840. [CrossRef]
101. Gombotz, M.; Pregartner, V.; Hanzu, I.; Wilkening, H.M.R. Fluoride-Ion Batteries: On the Electrochemical Stability of Nanocrystalline $La_{0.9}Ba_{0.1}F_{2.9}$ against Metal Electrodes. *Nanomaterials* **2019**, *9*, 1517. [CrossRef]
102. Sun, G.; Wang, H.; Jiang, Z. Humidity Response Properties of a Potentiometric Sensor Using LaF_3 Thin Film as the Solid Electrolyte. *Rev. Sci. Instrum.* **2011**, *82*, 083901. [CrossRef]
103. Moritz, W.; Fillipov, V.; Vasiliev, A.; Cherkashinin, G.; Szeponik, J. A Field Effect Based Hydrogen Sensor for Low and High Concentrations. *ECS Trans.* **2006**, *3*, 223. [CrossRef]
104. Sasidharan, S.; Aswathy, J.; Sajid, F.; Manzoor, K.; Shantikumar, N.; Deepthy, M. Ambient Temperature Synthesis of Citrate Stabilized and Biofunctionalized, Fluorescent Calcium Fluoride Nanocrystals for Targeted Labeling of Cancer Cells. *Biomater. Sci.* **2012**, *1*, 294–305. [CrossRef]